



Genome-wide screening reveals producer-cell modifications that improve virus-like particle production and delivery potency

Received: 2 February 2026

Accepted: 1 April 2026

Published online: 24 April 2026


 Check for updatesDiana Ly¹, Hyewon Jang¹, Adhiraj Goel¹, Arnav Singh¹ & Aditya Raguram^{1,2}  

Engineered virus-like particles (eVLPs) are promising vehicles for transient delivery of gene editing agents. While extensive particle engineering has yielded efficient eVLPs, it remains underexplored whether engineering the cells used to produce eVLPs could further improve eVLP properties. We report an unbiased genome-wide screening approach to systematically investigate how genetic perturbations in producer cells influence eVLP production. This approach generates eVLPs loaded with guide RNAs that identify the genetic perturbation in the cell that produced a particular particle; the abundance of each guide RNA in eVLPs therefore reflects how the corresponding genetic perturbation influences eVLP production or cargo loading. We apply this approach to identify several genes that regulate eVLP cargo expression and loading into particles during the production process. Leveraging these insights, we engineer producer cells that support increased eVLP cargo packaging and a 2- to 9-fold increase in eVLP delivery potency across several cargo, particle, and target-cell types in cultured cells and in mice. Our findings suggest the potential of producer-cell engineering as a useful strategy for improving the utility of eVLPs and related delivery methods.

Methods for safely and efficiently delivering macromolecules into cells in culture (in vitro) and within the body (in vivo) are required for many therapeutic strategies, including gene editing therapies^{1–5}. Recently, virus-like particles (VLPs) have emerged as promising vehicles for therapeutic macromolecule delivery that combine key advantages of canonical viral and non-viral delivery strategies^{1,6}. In typical VLPs, viral scaffold proteins are used to package and deliver cargo proteins, ribonucleoproteins (RNPs), or mRNAs instead of viral genetic material, which leads to transient cargo delivery into recipient cells^{1,6}. Several VLP-based delivery methods have proven particularly effective for gene editing applications^{7–23} and offer an ideal combination of efficient on-target editing, minimal off-target editing, and programmable cell-type targeting capabilities. Current state-of-the-art VLPs, including engineered VLPs (eVLPs)^{7,8,22}, have achieved efficient in vitro gene editing in primary human cells and therapeutic in vivo gene editing in the mouse liver and retina, highlighting the

utility of eVLP delivery for research and potential therapeutic applications.

While extensive engineering of eVLP components and particle architectures has afforded efficient eVLPs^{7,8,22}, further improvements to eVLP properties are still required to maximize their utility. In particular, improving eVLP cargo packaging per particle or overall particle yield from the eVLP production process would enable more efficient gene editing with lower eVLP doses and simplify the production of eVLPs for large-scale studies. Standard methods for producing eVLPs involve the use of human producer cells to express eVLP components and assemble functional particles^{7,8,22}, suggesting that producer cells likely play an important role in the eVLP production process. Indeed, producer-cell engineering has previously been used to improve the production of lentiviral vectors and adeno-associated viral vectors^{24–29}. However, previous studies have focused solely on particle engineering to improve eVLP properties, and none have explored whether

¹Whitehead Institute for Biomedical Research, Cambridge, MA, USA. ²Merkin Institute for Transformative Technologies in Healthcare, Broad Institute of MIT and Harvard, Cambridge, MA, USA.  e-mail: araguram@wi.mit.edu

producer-cell engineering could improve eVLP properties beyond what can be achieved through particle engineering alone.

In this study, we systematically investigate how genetic perturbations in producer cells influence eVLP production and apply our findings to improve eVLP production and delivery potency. Using an unbiased genome-wide screening approach in which eVLP-packaged guide-RNA cargos directly correspond to producer-cell genetic perturbations, we identify several genes that impact eVLP production, including genes that are uniquely relevant for packaging RNP cargos into genome-free eVLPs. Guided by these observations, we engineer producer cells that support improved eVLP production and delivery potency across several cargo, particle, and target-cell types in cultured cells and in mice. Our results lay a foundation for using producer-cell engineering to improve the utility of eVLPs and related bioparticle-based delivery methods.

Results

Genome-wide screening reveals producer-cell perturbations that influence eVLP production

We began by developing an unbiased genome-wide screening approach to identify genetic perturbations in producer cells that influence eVLP production (Fig. 1a). We envisioned a general scheme in which eVLP production is initiated from a pool of genetically perturbed producer cells. Each producer cell in this pool expresses a Cas9-based genome modifying agent and a single copy of a guide RNA (sgRNA) that directs the installation of a specific genetic perturbation

into that particular cell (Fig. 1a). Because eVLPs package Cas9-based cargos, the perturbation-inducing sgRNA expressed in a given producer cell is also loaded into any particles produced by that particular cell (Fig. 1a). Therefore, the abundance of a particular sgRNA in eVLPs reflects how the corresponding genetic perturbation influences eVLP production or cargo loading: sgRNAs that are more abundant identify perturbations that increase eVLP production or cargo loading, while sgRNAs that are less abundant identify perturbations that decrease eVLP production or cargo loading (Fig. 1a).

We used this general approach to perform a genome-wide knockout screen for cargo-loaded eVLP production in Gesicle 293T producer cells, a standard cell line used for eVLP production^{7,8,22}. We transduced producer cells at a low multiplicity of infection (MOI) with a lentiviral sgRNA library containing 98,077 unique sgRNAs targeting 19,707 genes across the human genome³⁰ (Supplementary Fig. 1a). Each vector in the library also encoded constitutive expression of Cas9 nuclease. After selecting for Cas9 expression and expanding the transduced cells to generate a pool of single-knockout producer cells, we initiated fourth-generation (v4) adenine base editor (ABE)-eVLP production from these cells (Supplementary Fig. 1a). Importantly, to initiate eVLP production, we only transfected plasmids encoding the expression of v4 ABE-eVLP protein components: (1) the gag-ABE (capsid-cargo) fusion, (2) the Moloney murine leukemia virus (MMLV) gag-pro-pol polyprotein, and (3) the vesicular stomatitis virus G (VSV-G) envelope protein. No additional sgRNA-encoding plasmid was transfected, ensuring that all eVLPs produced from a given producer

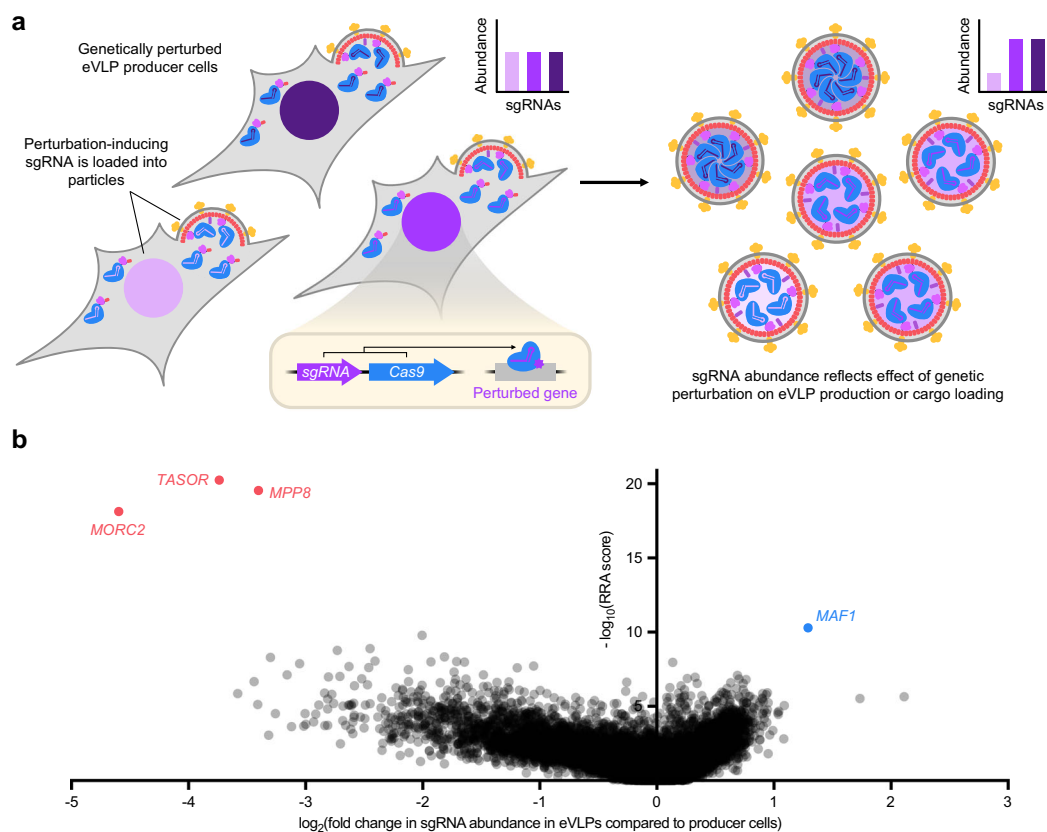


Fig. 1 | Genome-wide screening reveals genetic perturbations that influence eVLP production. **a** Overview of the producer-cell screening approach. eVLP production is initiated from a pool of genetically perturbed producer cells, and each eVLP packages sgRNAs that identify the specific genetic perturbation in the cell that produced that particular eVLP. The abundance of a particular sgRNA in eVLPs compared to producer cells reflects how the corresponding genetic perturbation influences eVLP production or cargo loading. Some images were created in BioRender. Raguram, A. (2026) <https://BioRender.com/lwbkh2r>. **b** Gene-level

phenotypes from the genome-wide knockout screen for cargo-loaded eVLP production. Each gene is represented as a single dot whose x-coordinate reflects the median fold change in sgRNA abundance in eVLPs compared to producer cells for all sgRNAs targeting that particular gene, and whose y-coordinate reflects the MAGeCK RRA score associated with that particular gene (see “Methods”). Data reflect $n = 2$ screen replicates. See also Supplementary Fig. 1c and Supplementary Data 6. Source data are provided as a Source Data file.

cell packaged cargo containing the specific knockout-inducing sgRNA that was already introduced into that producer cell by lentiviral transduction (Fig. 1a and Supplementary Fig. 1a).

Following eVLP production, we isolated RNA from purified eVLPs and compared this eVLP-packaged RNA to cellular RNA that was isolated from the single-knockout producer-cell pool immediately prior to eVLP production (Fig. 1a and Supplementary Fig. 1a). To compare sgRNA abundances across both populations, we subjected both RNA pools to template-switching reverse transcription³¹, which enabled amplification and sequencing of the spacer sequence at the 5' end of each sgRNA molecule (Supplementary Fig. 1b). sgRNAs that are more abundant in the eVLP-packaged RNA compared to the producer-cell RNA identify gene knockouts that increase eVLP production or cargo loading, while sgRNAs that are less abundant identify gene knockouts that decrease eVLP production or cargo loading (Fig. 1a and Supplementary Fig. 1a).

By aggregating the results for all sgRNAs targeting the same gene into gene-level phenotypes, we determined the effect of each producer-cell gene knockout on eVLP production or cargo loading (Fig. 1b and Supplementary Fig. 1c). We observed that the majority of gene knockouts did not substantially impact eVLP production or cargo loading, some knockouts decreased eVLP production or cargo loading, and very few knockouts increased eVLP production or cargo loading (Fig. 1b). These results are consistent with a model in which there are more genes in producer cells that positively regulate eVLP production than genes that negatively regulate eVLP production. Taken together, the results of this genome-wide knockout screen illuminate the producer-cell determinants of eVLP production and nominate several gene knockouts ("hits") that appear to strongly impact eVLP production or cargo loading (Fig. 1b).

Knockout of HUSH-associated genes negatively impacts eVLP sgRNA packaging in the presence of lentiviral Cas9 expression

Next, we sought to characterize the gene knockouts that most strongly decreased eVLP production or cargo loading. While these negative hits might not be immediately applicable for improving eVLP manufacturing, we reasoned that characterizing these gene knockouts would reveal important insights into how producer-cell factors influence eVLPs, which could inform alternative strategies for improving eVLP production. The three strongest negative hits from our screen—*MPP8*, *TASOR*, and *MORC2*—are all associated with the human silencing hub (HUSH) complex, which is responsible for epigenetically silencing intronless transgenes, including retroviral elements^{32,33}. We first individually validated each negative hit by measuring the relative sgRNA abundance in eVLPs produced from *MPP8*-, *TASOR*-, or *MORC2*-knockout cells (hereafter collectively referred to as HUSH-knockout cells) compared to eVLPs produced from standard producer cells. To independently generate each knockout cell line, we mimicked the screen conditions and transduced Gesicle cells with a lentiviral vector encoding constitutive expression of Cas9 nuclease and an appropriate targeting sgRNA, selected cells for Cas9 expression, and isolated a polyclonal population of Cas9-edited cells (Supplementary Fig. 2a). To control for the effects of Cas9 expression and Cas9 nuclease-mediated indel generation on producer cells, we also applied the same procedure to generate modified Gesicle cells using a sgRNA targeting *AAVSI*, a human safe harbor locus³⁴. After knockout generation, we initiated v4 ABE-eVLP production from each cell line by transfecting plasmids encoding the expression of all required components, including a sgRNA targeting the human *BCL11A* +58 enhancer locus³⁵ (Supplementary Fig. 2a). We detected by RT-qPCR a 1.5- to 3.8-fold decrease in sgRNA abundance in ABE-eVLPs produced from HUSH-knockout cells compared to ABE-eVLPs produced from *AAVSI*-knockout cells (Fig. 2a), confirming the results of our screen. Additionally, when we transduced HEK293T cells with a range of doses of purified ABE-eVLPs and measured adenine base editing efficiencies at the *BCL11A* +58 enhancer

target locus via high-throughput sequencing (Supplementary Fig. 2a), we observed that ABE-eVLPs produced from HUSH-knockout cells exhibited a 2.3- to 4.4-fold decrease in in vitro delivery potency (EC_{50}) compared to ABE-eVLPs produced from *AAVSI*-knockout cells (Fig. 2b). These results indicate that knockout of HUSH-associated genes *MPP8*, *TASOR*, or *MORC2* in producer cells negatively impacts eVLP production or cargo loading.

We hypothesized that these HUSH-associated genes might impact eVLP production or cargo loading by modulating the expression of the lentivirally integrated Cas9 nuclease that was used to generate the gene knockouts. To test this hypothesis, we measured the relative abundance of Cas9 mRNA or protein in each knockout cell line by RT-qPCR or Western blot, respectively. We observed a 5.4- to 29-fold increase in cellular Cas9 mRNA expression and a 10- to 14-fold increase in Cas9 protein expression in HUSH-knockout cells compared to *AAVSI*-knockout cells (Fig. 2c, d and Supplementary Fig. 3a). These results suggest a model in which HUSH-associated gene products natively silence lentivirally integrated Cas9 expression in *AAVSI*-knockout producer cells, but in HUSH-knockout cells, Cas9 is no longer efficiently silenced (Supplementary Fig. 3b). Therefore, during eVLP production, excess Cas9 protein in HUSH-knockout producer cells likely competes for sgRNA binding and prevents sgRNA molecules from efficiently binding to gag-ABE, which ultimately decreases both sgRNA packaging into eVLPs and eVLP delivery potency (Supplementary Fig. 3b). To further investigate this phenomenon, we used v4 Cas9-eVLP transduction instead of Cas9/sgRNA lentiviral transduction to generate HUSH-knockout Gesicle cells that lacked any integrated Cas9 transgene (Supplementary Fig. 2b). Notably, we did not detect any change in sgRNA abundance by RT-qPCR in ABE-eVLPs produced from these Cas9-free HUSH-knockout cells compared to standard producer cells (Supplementary Fig. 4a). These results suggest that, consistent with our model above, both lentivirally integrated Cas9 expression and knockout of HUSH-associated genes are required to decrease sgRNA abundance in eVLPs. Collectively, these data and our proposed model rationalize the negative performance of HUSH-associated gene knockouts in our screen.

Knockout of HUSH-associated genes increases eVLP protein cargo expression

Interestingly, we noticed that ABE-eVLPs produced from Cas9-free HUSH-knockout cells still exhibited a 2.6- to 3.9-fold decrease in delivery potency compared to ABE-eVLPs produced from standard Gesicle cells (Supplementary Fig. 4b), suggesting that some eVLP property other than sgRNA abundance was negatively impacted due to Cas9-free HUSH-associated gene knockout. We hypothesized that these HUSH-associated genes might also modulate the expression of eVLP components from plasmids transfected during the eVLP production process. To investigate this possibility, we performed Western blots to quantify eVLP cargo (gag-ABE) expression in producer cells following transfection of eVLP production plasmids, which revealed a 2.1- to 4.4-fold increase in gag-ABE protein expression in HUSH-knockout cells compared to Gesicle cells (Supplementary Fig. 4c, d). We reasoned that this increase in eVLP cargo expression might disrupt the optimal eVLP component stoichiometry (gag-ABE:gag-pro-pol ratio), which was previously found to be an important determinant of eVLP potency⁸. Consistent with this model, we observed that reducing the transfected gag-ABE:gag-pro-pol plasmid ratio from 25:75 to 10:90 or 5:95 restored the potency of ABE-eVLPs produced from *MORC2*-knockout cells back to standard levels (Supplementary Fig. 4e). These results indicate that the increase in eVLP cargo expression in HUSH-knockout producer cells and corresponding disruption of the optimal eVLP component stoichiometry can be counteracted simply by reducing the amount of transfected eVLP cargo plasmid, thereby effectively restoring the optimal stoichiometry.

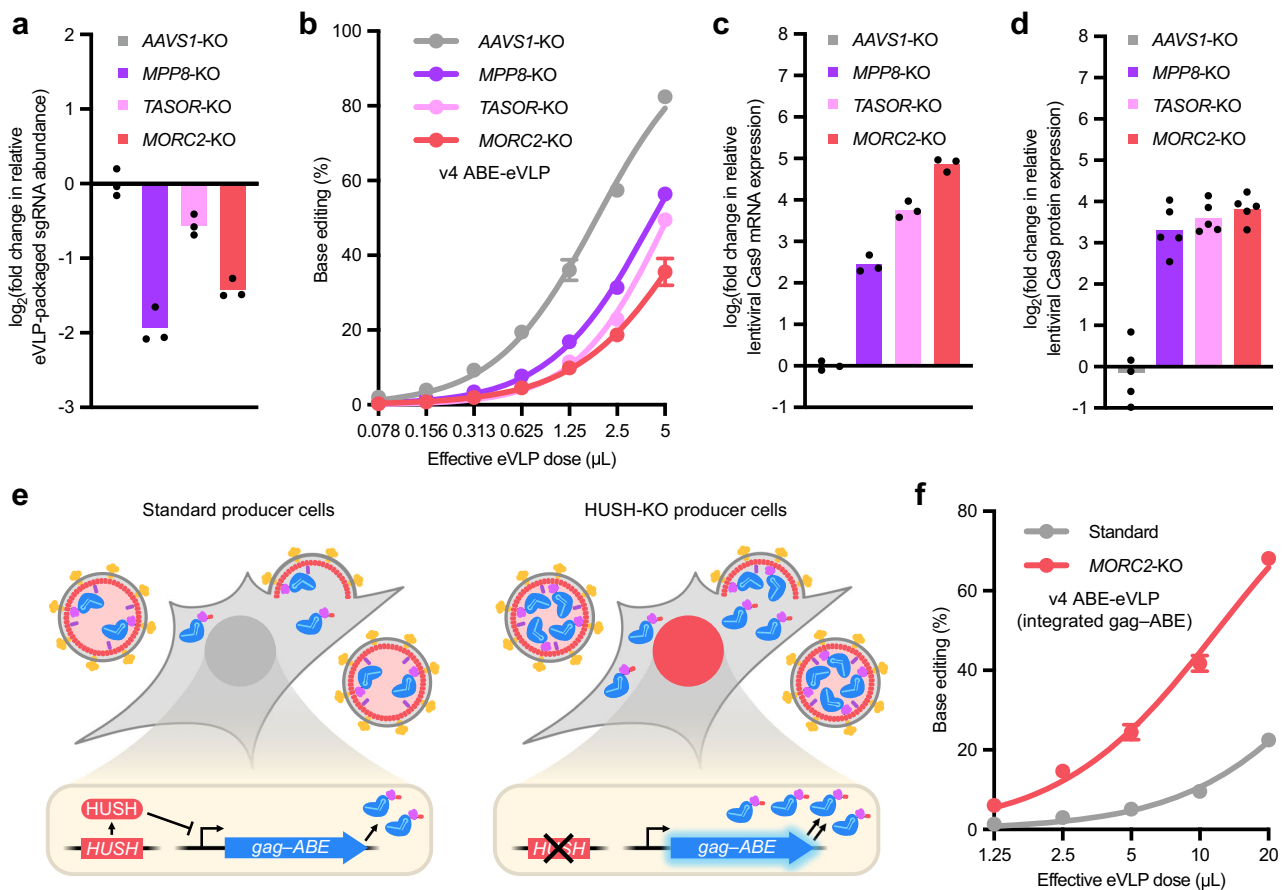


Fig. 2 | Knockout of HUSH-associated genes influences eVLP sgRNA packaging, protein cargo expression, and delivery potency. **a** Fold change in eVLP-packaged sgRNA abundance measured by RT-qPCR, normalized relative to sgRNA abundance in eVLPs produced from *AAVS1*-knockout cells. Bars reflect the mean of $n = 3$ replicates, and dots represent individual replicate values. **b** Comparison of v4 ABE-eVLPs produced from *AAVS1*-knockout or HUSH-knockout cells across a range of eVLP doses. Adenine base editing efficiencies at position A_7 of the *BCL11A* +58 enhancer site in HEK293T cells are shown. **c** Fold change in producer-cell Cas9 mRNA abundance measured by RT-qPCR, normalized relative to Cas9 mRNA abundance in *AAVS1*-knockout cells. Bars reflect the mean of $n = 3$ replicates, and dots represent individual replicate values. **d** Fold change in producer-cell Cas9 protein abundance measured by Western blot, normalized relative to Cas9 protein abundance in *AAVS1*-knockout cells. Bars reflect the mean of $n = 5$ replicates, and

dots represent individual replicate values. See also Supplementary Fig. 3a. **e** Schematic of standard producer cells versus HUSH-knockout producer cells, both containing genomically integrated *gag*-ABE expression cassettes. In standard cells, epigenetic silencing by the HUSH complex limits *gag*-ABE expression. In HUSH-knockout cells, lack of HUSH-mediated silencing leads to increased *gag*-ABE expression and loading into eVLPs. Some images were created in BioRender. Raguram, A. (2026) <https://BioRender.com/lwbkh2r>. **f** Comparison of v4 ABE-eVLPs produced from standard or *MORC2*-knockout Gesicle cells, both containing genomically integrated *gag*-ABE expression cassettes. Adenine base editing efficiencies at position A_5 of the *HEK2* site in HEK293T cells are shown. **b, f** Dots and error bars represent mean \pm s.d. of $n = 3$ biological replicates. Data were fit to four-parameter logistic curves using nonlinear regression. Source data are provided as a Source Data file.

Given our finding that knockout of HUSH-associated genes increases eVLP cargo expression, we wondered whether HUSH-knockout producer cells could in fact improve eVLP production in specific contexts. In particular, certain applications of eVLPs, including our recently described barcoded eVLP evolution system²², require expressing *gag*-ABE from genomically integrated cassettes rather than transfected plasmids, which results in reduced *gag*-ABE protein levels and suboptimal component stoichiometry. We reasoned that the use of HUSH-knockout producer cells should increase *gag*-ABE expression from genomically integrated cassettes, which in this case would improve rather than disrupt the eVLP component stoichiometry (Fig. 2e). Consistent with this model, we observed that ABE-eVLPs produced from *MORC2*-knockout cells with integrated *gag*-ABE expression exhibited a 4.6-fold increase in delivery potency compared to ABE-eVLPs produced from standard cells with integrated *gag*-ABE expression (Fig. 2f). These results indicate that HUSH-knockout producer cells support improved eVLP delivery potency in situations in which *gag*-cargo expression is limiting. Altogether, our results reveal a previously unknown role for HUSH-

associated genes in modulating eVLP cargo expression in producer cells and highlight the importance of optimizing eVLP cargo expression and component stoichiometry to maximize eVLP potency.

MAF1-knockout producer cells improve sgRNA packaging into eVLPs

Next, we sought to characterize the gene knockouts from our screen that most strongly increased eVLP production or cargo loading. The single strongest positive hit from our screen was *MAF1*, a repressor of RNA Pol III transcription^{36–38}. Because all sgRNAs in our experiments were expressed from an RNA Pol III-transcribed U6 promoter, we reasoned that knockout of *MAF1* in producer cells likely leads to increased sgRNA transcription and loading into eVLP-packaged cargos (Fig. 3a).

To test this hypothesis, after generating *MAF1*-knockout Gesicle cells using v4 Cas9-eVLPs (Supplementary Fig. 2b), we initiated v4 ABE-eVLP production from these cells by transfecting plasmids encoding the expression of all required components. We detected by RT-qPCR a

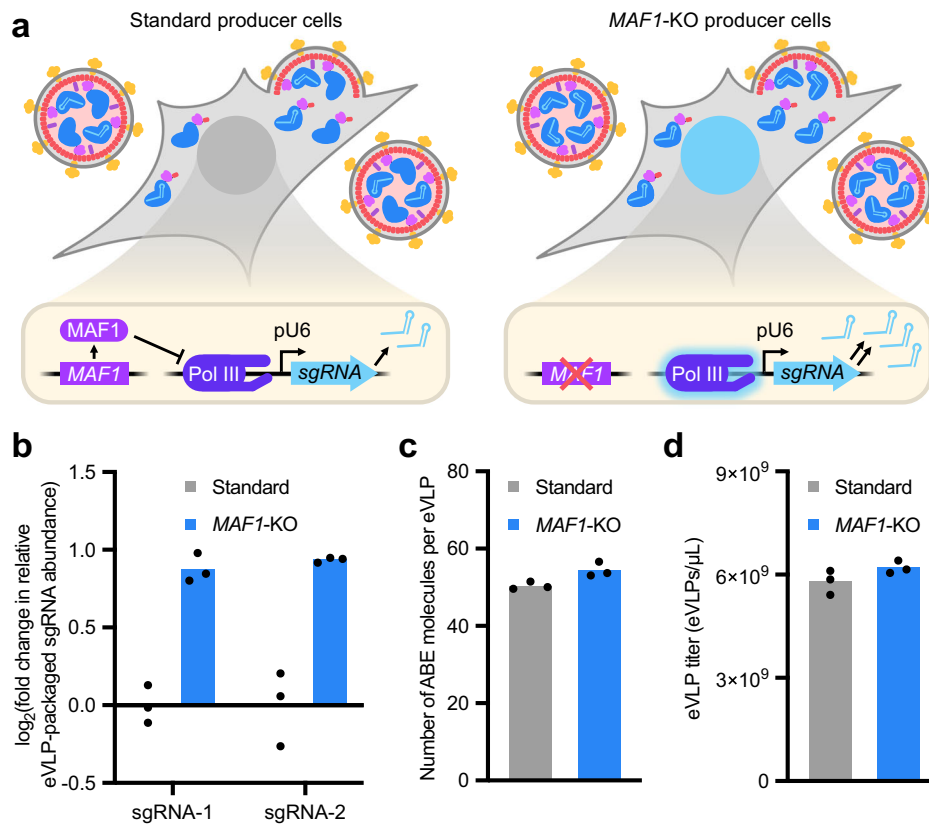


Fig. 3 | *MAF1*-knockout producer cells improve eVLP sgRNA packaging.

a Schematic of standard producer cells versus *MAF1*-knockout producer cells. In standard cells, *MAF1* represses RNA Pol III transcription, which limits producer-cell sgRNA expression. In *MAF1*-knockout producer cells, RNA Pol III is no longer subjected to *MAF1*-mediated repression, which increases sgRNA expression and loading into eVLP-packaged RNPs. Some images were created in BioRender. Raguram, A. (2026) <https://BioRender.com/lwbkh2r>. **b** Fold change in eVLP-

packaged sgRNA abundance measured by RT-qPCR, normalized relative to sgRNA abundance in eVLPs produced from standard Gesicle cells. sgRNA-1 and sgRNA-2 denote two different packaged sgRNA sequences. **c, d** Quantification of ABE molecules per eVLP (**c**) and eVLP particle titer (**d**) by anti-Cas9 and anti-MLV p30 ELISA (see “Methods”). **b–d** Bars reflect the mean of $n = 3$ replicates, and dots represent individual replicate values. Source data are provided as a Source Data file.

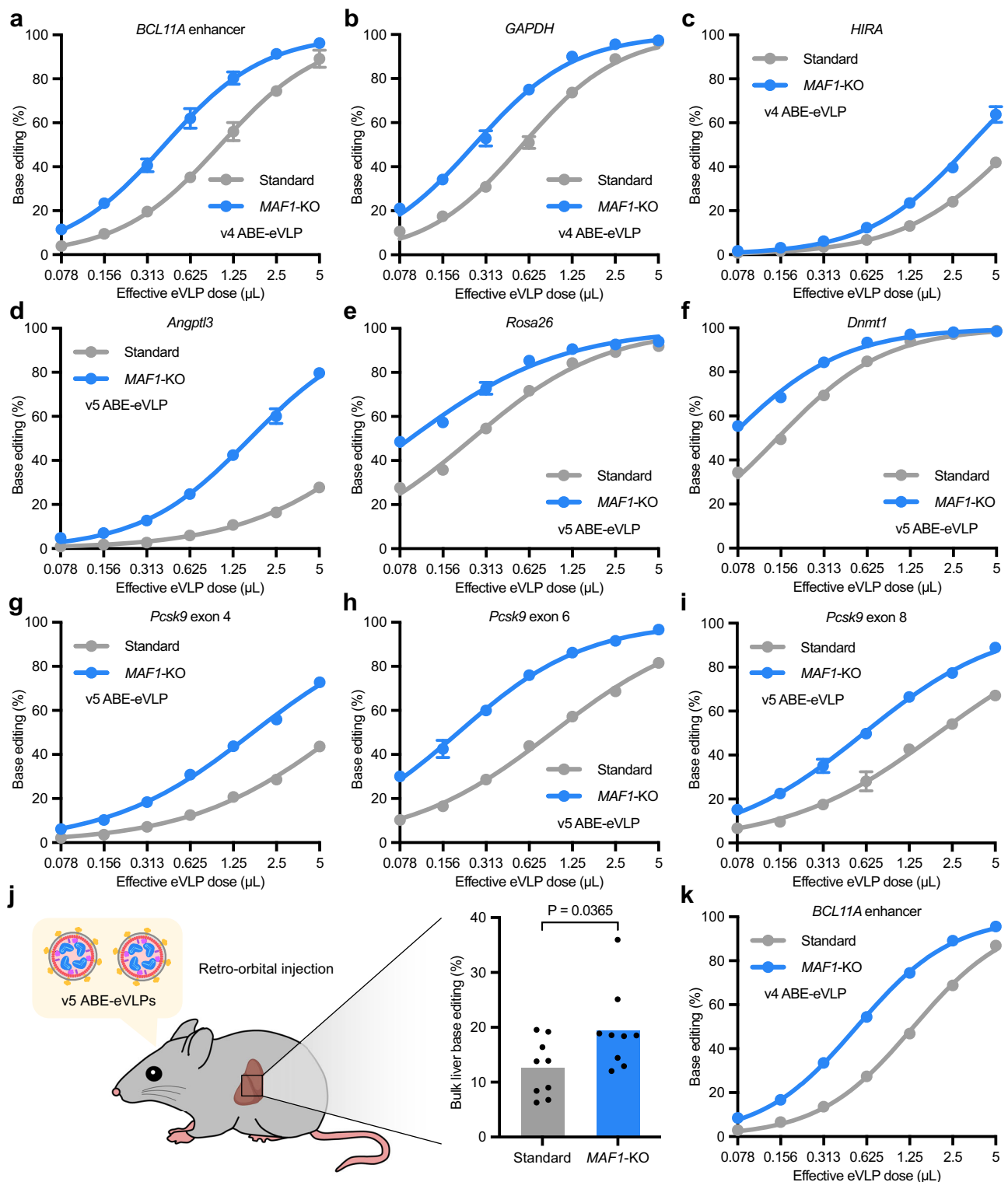
2-fold increase in sgRNA abundance in ABE-eVLPs produced from *MAF1*-knockout cells compared to ABE-eVLPs produced from standard Gesicle cells (Fig. 3b). Additionally, we observed that ABE-eVLPs produced from *MAF1*-knockout cells packaged similar numbers of ABE cargo proteins per particle and were produced at similar particle titers compared to ABE-eVLPs produced from standard Gesicle cells (Fig. 3c, d), suggesting that the use of *MAF1*-knockout cells increases sgRNA packaging alone without affecting protein packaging or particle yield. Collectively, these data confirm our knockout screen results and indicate that *MAF1*-knockout producer cells support increased sgRNA loading into eVLPs.

MAF1-knockout producer cells support improved eVLP delivery potency in cultured cells and in mice

Because increased sgRNA loading leads to an increased number of active RNP cargo molecules packaged into eVLPs (Fig. 3a), we reasoned that ABE-eVLPs produced from *MAF1*-knockout cells should exhibit increased delivery potency compared to ABE-eVLPs produced from standard Gesicle cells. Encouragingly, we observed that v4 ABE-eVLPs produced from *MAF1*-knockout cells exhibited a 2.5-fold increase in delivery potency (EC_{50}) at the *BCL11A*+58 enhancer locus in HEK293T cells compared to v4 ABE-eVLPs produced from standard Gesicle cells (Fig. 4a). v4 ABE-eVLPs produced from *MAF1*-knockout cells also exhibited a 2.2- and 2.1-fold increase in delivery potency at the *GAPDH* and *HIRA* genomic loci in HEK293T cells, respectively (Fig. 4b, c), indicating that the eVLP potency improvement conferred by the use of *MAF1*-knockout producer cells is not restricted to any

particular sgRNA sequence or target genomic locus. Additionally, we assessed whether the use of *MAF1*-knockout producer cells could also improve the delivery potency of the more recently developed v5 ABE-eVLPs, which use laboratory evolved capsid proteins that were optimized to improve BE RNP cargo packaging²². We observed that v5 ABE-eVLPs produced from *MAF1*-knockout cells exhibited a 2.2- to 9.1-fold increase in delivery potency compared to v5 ABE-eVLPs produced from standard cells across six distinct target genomic loci in mouse Neuro-2a cells (Fig. 4d–i). Together, these results indicate that the increased sgRNA packaging in ABE-eVLPs produced from *MAF1*-knockout cells leads to corresponding improvements in eVLP delivery potency in vitro.

To further explore the utility of *MAF1*-knockout producer cells, we investigated whether their use could also improve in vivo eVLP delivery efficiencies. We produced v5 ABE-eVLPs targeting the *Pcsk9* exon 1 splice donor^{8,39} using either standard or *MAF1*-knockout Gesicle cells, and we injected these ABE-eVLPs retro-orbitally into adult mice at a low, sub-saturating eVLP dose (Fig. 4j). We observed that v5 ABE-eVLPs produced from *MAF1*-knockout cells achieved 19.4% average in vivo base editing at the *Pcsk9* locus in bulk liver tissue, while v5 ABE-eVLPs produced from standard cells administered at the same dose only achieved 12.6% bulk liver editing (Fig. 4j, $P = 0.0365$, two-sided unpaired t test). Collectively, these data indicate that *MAF1*-knockout producer cells support improved eVLP potency across different target genomic loci and target-cell types both in vitro and in vivo, demonstrating the benefits of using *MAF1*-knockout cells instead of standard cells for eVLP production.



MAFI-knockout producer cells support improved delivery potency across various cargo, particle, and producer-cell types

We next sought to further evaluate the ability of *MAFI*-knockout producer cells to support improved eVLP production and potency in other various contexts. First, we investigated whether knockdown of *MAFI* could improve eVLP production from HEK293T/17 cells, another cell line that is commonly used for viral vector production^{8,22,40}. Following the generation of *MAFI*-knockout HEK293T/17 cells using v4 Cas9-eVLPs, we observed that v4 ABE-eVLPs produced from *MAFI*-knockout HEK293T/17 cells exhibited a 2.5-fold increase in in vitro delivery

potency compared to those produced from standard HEK293T/17 cells (Fig. 4k). These results indicate that the improvements conferred by *MAFI* knockout are generalizable beyond the specific cell line (Gesicle 293T) in which our knockout screen was conducted. Additionally, our findings suggest that knockdown of *MAFI* might similarly benefit eVLP production from HEK293T/17 clones that have been adapted for growth in suspension culture, which are particularly well suited for large-scale bioparticle manufacturing⁴¹.

Second, we assessed whether *MAFI*-knockout producer cells could improve the potency of eVLPs that package different Cas9-

Fig. 4 | *MAF1*-knockout producer cells improve eVLP delivery potency in cultured cells and in mice. **a–c** Comparison of v4 ABE-eVLPs produced from standard or *MAF1*-knockout Gesicle cells across a range of eVLP doses in HEK293T cells. Adenine base editing efficiencies are shown at position A₇ of the *BCL11A* +58 enhancer site (**a**), position A₇ of the *GAPDH* site (**b**), and position A₅ of the *HIRA* site (**c**). **d–i** Comparison of v5 ABE-eVLPs produced from standard or *MAF1*-knockout Gesicle cells across a range of eVLP doses in mouse Neuro-2a cells. Adenine base editing efficiencies are shown at position A₈ of the *Angptl3* exon 7 splice acceptor site (**d**), position A₄ of the *Rosa26* site (**e**), position A₉ of the *Dnmt1* site (**f**), position A₆ of the *Pcsk9* exon 4 splice acceptor site (**g**), position A₄ of the *Pcsk9* exon 6 splice donor site (**h**), and position A₈ of the *Pcsk9* exon 8 splice acceptor site (**i**). **j** Schematic of mouse experiments and adenine base editing efficiencies at position

A₆ of the *Pcsk9* exon 1 splice donor site in bulk mouse liver tissue. Each mouse was injected with 15 μ L of 1500-fold concentrated purified v5 ABE-eVLPs containing 3×10^{11} eVLPs as determined by anti-MLV p30 ELISA (see “Methods”). Bars reflect the mean of $n = 9$ mice per condition, and dots represent individual mouse values. *P* value was calculated using a two-sided unpaired *t* test. Some images were created in BioRender. Raguram, A. (2026) <https://BioRender.com/lwbkh2r>. **k** Comparison of v4 ABE-eVLPs produced from standard or *MAF1*-knockout HEK293T/17 cells across a range of eVLP doses in HEK293T cells. Adenine base editing efficiencies at position A₇ of the *BCL11A* +58 enhancer site are shown. **a–i, k** Dots and error bars represent mean \pm s.d. of $n = 4$ (**a**) or $n = 3$ (**b–i, k**) biological replicates. Data were fit to four-parameter logistic curves using nonlinear regression. Source data are provided as a Source Data file.

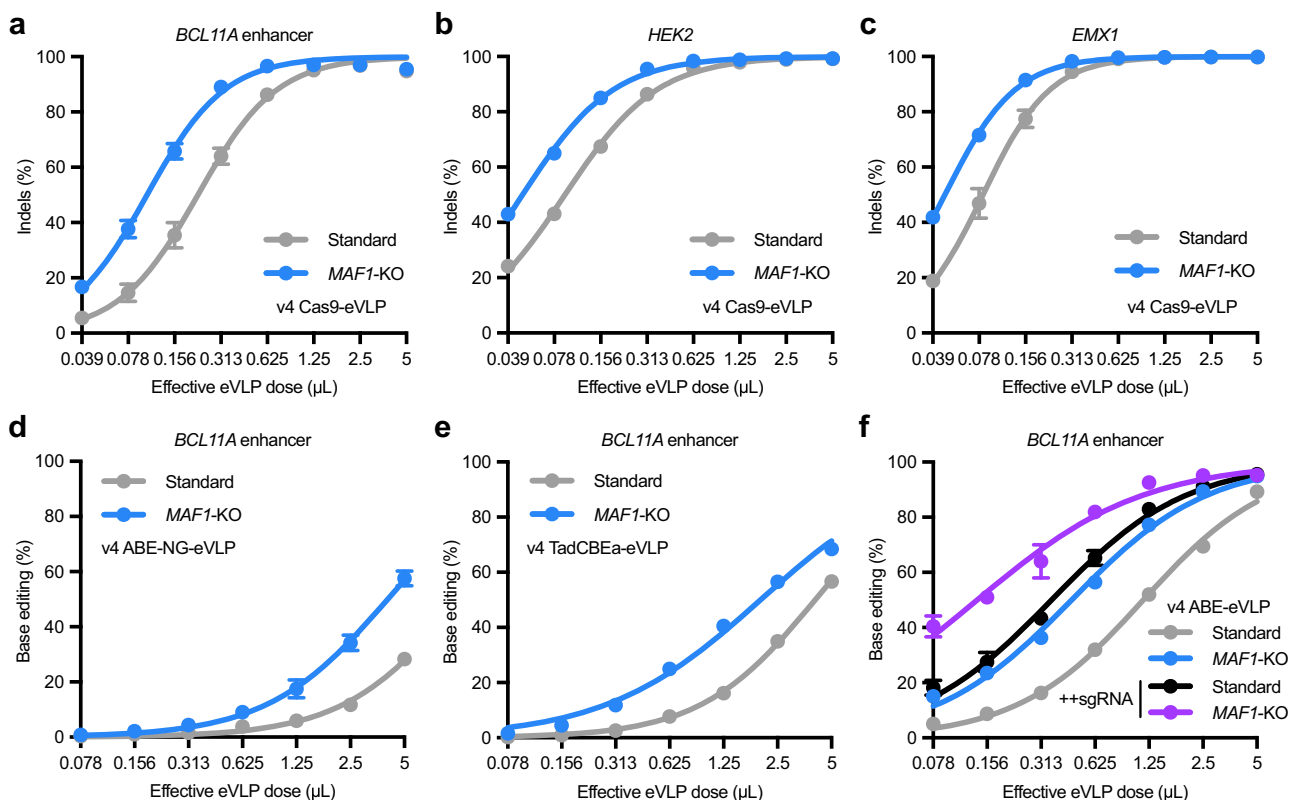


Fig. 5 | *MAF1*-knockout producer cells improve eVLP delivery potency across cargo types. **a–c** Comparison of v4 Cas9-eVLPs produced from standard or *MAF1*-knockout Gesicle cells across a range of eVLP doses in HEK293T cells. Indel frequencies are shown at the *BCL11A* +58 enhancer site (**a**), *HEK2* site (**b**), and *EMX1* site (**c**). **d** Comparison of v4 ABE-NG-eVLPs produced from standard or *MAF1*-knockout Gesicle cells across a range of eVLP doses. Adenine base editing efficiencies at position A₇ of the *BCL11A* +58 enhancer site in HEK293T cells are shown. **e** Comparison of v4 TadCBEa-eVLPs produced from standard or *MAF1*-knockout Gesicle cells across a range of eVLP doses. Cytosine base editing efficiencies at

position C₆ of the *BCL11A* +58 enhancer site in HEK293T cells are shown. **f** Comparison of v4 ABE-eVLPs or v4 ABE-eVLPs with additional sgRNA-expressing plasmids (++sgRNA, see Supplementary Fig. 7) produced from standard or *MAF1*-knockout Gesicle cells across a range of eVLP doses. Adenine base editing efficiencies at position A₇ of the *BCL11A* +58 enhancer site in HEK293T cells are shown. **a–f** Dots and error bars represent mean \pm s.d. of $n = 4$ (**d**) or $n = 3$ (**a–c, e, f**) biological replicates. Data were fit to four-parameter logistic curves using nonlinear regression. Source data are provided as a Source Data file.

based RNP cargos. We observed that v4 eVLPs packaging either Cas9 nuclease, ABE-SpCas9-NG⁴², or TadCBEa⁴³ cargos exhibited a 2.0- to 2.5-fold improvement in delivery potency when produced from *MAF1*-knockout cells compared to Gesicle cells (Fig. 5a–e).

Third, we explored whether *MAF1*-knockout producer cells could also improve the performance of non-eVLP delivery vehicles, including several recently reported RNP-packaging VLP- and vesicle-based systems. We evaluated four different non-eVLP systems that use various particle scaffolds and cargo loading mechanisms (Supplementary Fig. 5a): (1) ENVLPE⁺ (engineered nucleocytoplasmic vehicles for loading of programmable editors)¹⁰, (2) miniEDV (minimal enveloped delivery vehicles)⁴⁴, (3) RIDE VLPs¹⁶, and (4) VEDIC (VSV-G plus EV-Sorting

Domain-Intein-Cargo)⁴⁵ particles. We observed that ABE-packaging ENVLPE⁺ particles produced from *MAF1*-knockout cells exhibited a 2.2-fold increase in delivery potency compared to the same particles produced from standard Gesicle cells, which was nearly identical to the improvement we observed for v4 ABE-eVLPs (Supplementary Fig. 5b, c). Prime editor (PE)-packaging ENVLPE⁺ particles produced from *MAF1*-knockout cells also exhibited a 2.1-fold increase in delivery potency compared to the same particles produced from standard Gesicle cells (Supplementary Fig. 5d). Additionally, we observed that Cas9-packaging miniEDVs, ABE-packaging RIDE VLPs, and Cas9-packaging VEDIC particles produced from *MAF1*-knockout cells exhibited a 1.7-, 1.8-, and 2.6-fold increase in delivery potency,

respectively, compared to the same particles produced from standard Gesicle cells (Supplementary Fig. 5e–g). These results indicate that the improvements conferred by *MAFI*-knockout producer cells are generalizable across several different RNP-packaging cell-derived bioparticles that use distinct particle scaffolds and cargo packaging mechanisms. Taken together, our findings demonstrate that knockout of *MAFI* in producer cells yields consistent improvements in VLP delivery potency across eVLP cargo types, particle types, and producer-cell lines.

***MAFI*-knockout producer cells improve sgRNA packaging into eVLPs across different sgRNA expression levels**

Finally, we evaluated whether the improvements conferred by *MAFI*-knockout cells could synergize with additional strategies for modulating sgRNA expression levels in producer cells. We observed that increasing the ratio of sgRNA-expressing plasmid to other packaging plasmids transfected during eVLP production did not improve the delivery potency of v4 ABE-eVLPs produced from either standard Gesicle cells or *MAFI*-knockout cells (Supplementary Fig. 6a, b). Increasing the absolute amount of sgRNA-expressing plasmid transfected during eVLP production by up to twofold also did not improve the delivery potency of v4 ABE-eVLPs produced from either standard Gesicle cells or *MAFI*-knockout cells (Supplementary Fig. 6c). These results indicate that simply increasing the amount of sgRNA-expressing plasmid transfected during eVLP production is not sufficient to improve eVLP potency, possibly because of tradeoffs associated with either reducing the amounts of other packaging plasmids or increasing the total amount of transfected DNA per producer cell.

To further investigate alternative strategies for improving sgRNA expression, we adopted a strategy that was recently developed for enveloped delivery vehicles (EDVs) in which additional sgRNA expression cassettes are included in the other packaging plasmids¹³ (Supplementary Fig. 7a). This strategy (hereafter referred to as ++sgRNA) avoids the tradeoffs mentioned above since the amount of sgRNA-encoding DNA is increased without substantially perturbing the amounts of other packaging plasmids or the total amount of transfected DNA per producer cell. We observed that v4 ABE-eVLPs produced from Gesicle cells using ++sgRNA plasmids exhibited a 3.3-fold increase in delivery potency compared to standard v4 ABE-eVLPs produced from Gesicle cells (Fig. 5f). Additionally, we observed that v4 ABE-eVLPs produced from *MAFI*-knockout cells using ++sgRNA plasmids also exhibited a 3.4-fold increase in delivery potency compared to standard v4 ABE-eVLPs produced from *MAFI*-knockout cells (Fig. 5f). These results indicate that the use of ++sgRNA plasmids synergizes with *MAFI*-knockout producer cells to further improve delivery potency. Importantly, v4 ABE-eVLPs produced using ++sgRNA plasmids still exhibited a 2.6-fold increase in delivery potency when produced from *MAFI*-knockout cells compared to Gesicle cells, highlighting the consistent benefit of using *MAFI*-knockout producer cells. Indeed, combining ++sgRNA plasmids and *MAFI*-knockout producer cells yielded the most potent eVLP-mediated base editing at the *BCL11A* enhancer site in HEK293T cells that we observed in this study (Fig. 5f).

We confirmed via RT-qPCR that both the ++sgRNA strategy and knockout of *MAFI* led to increased sgRNA packaging into eVLPs; these increases in sgRNA packaging were additive when both modified strategies were employed (Supplementary Fig. 7b). In particular, we observed that combining both strategies increased the percentage of eVLP-packaged Cas9 molecules complexed with sgRNAs from 20% to 50% (Supplementary Fig. 7b). Collectively, our findings demonstrate that the use of *MAFI*-knockout producer cells can further improve eVLP properties when combined with additional strategies for increasing sgRNA expression during eVLP production.

Discussion

In this study, we developed a general genome-wide screening approach to comprehensively evaluate how genetic perturbations in producer cells influence eVLP production. Using this approach, we identified the HUSH epigenetic silencing complex and the RNA Pol III repressor *MAFI* as key regulators of eVLP protein and sgRNA cargo expression, respectively. Leveraging these insights, we engineered HUSH-knockout producer cells that support a 4-fold increase in eVLP delivery potency when particles are produced using genomically integrated gag–cargo expression, and *MAFI*-knockout producer cells that support a 2- to 9-fold increase in eVLP delivery potency under standard production conditions across several cargo, particle, producer-cell, and target-cell types.

Our results reveal a previously underappreciated role for the HUSH complex in modulating eVLP protein cargo expression in producer cells. Under standard eVLP production conditions, we found that HUSH-knockout producer cells exhibited increased gag–cargo expression, which disrupted the optimal component stoichiometry and reduced eVLP potency. However, under conditions in which gag–cargo expression is limiting, including when particles are produced using genomically integrated gag–cargo expression, we found that the use of HUSH-knockout producer cells improved eVLP delivery potency (Fig. 2f). We therefore anticipate that HUSH-knockout producer cells will be useful for eVLP applications in which genomically integrated gag–cargo expression is required (e.g., barcoded eVLP evolution²²). Additionally, our results suggest that HUSH-knockout cells are likely to be valuable for future efforts to produce eVLPs or related particles using producer cells that stably express components from genomically integrated cassettes instead of transfected plasmids, a strategy that has proven useful for viral vector manufacturing^{27,46–48}.

We anticipate that the use of *MAFI*-knockout cells instead of standard producer cells will advance the utility of VLP delivery in several ways. For one, eVLPs produced from *MAFI*-knockout cells exhibit increased sgRNA packaging and increased delivery potency both in cultured cells and in mice compared to standard eVLPs (Fig. 4), suggesting that *MAFI*-knockout producer cells should be used when maximal editing efficiencies are required. Additionally, the gene editing efficiencies at a given dose of eVLPs produced from standard cells can in general be achieved using a 2- to 9-fold lower dose of eVLPs produced from *MAFI*-knockout cells (Fig. 4a–i), suggesting that using *MAFI*-knockout cells for eVLP production will be especially beneficial for applications that are constrained by the maximum administrable eVLP dose. Furthermore, by minimizing the eVLP dose required to achieve efficient editing, the use of *MAFI*-knockout producer cells would also reduce the total volume of producer-cell culture required for eVLP production, which could greatly simplify the application of eVLPs in large-scale studies. Importantly, given that several previous studies have identified sgRNA loading into VLPs and related delivery vehicles as a bottleneck that limits delivery potency^{8,13,22,49}, our discovery that *MAFI*-knockout producer cells improve sgRNA loading into VLPs will likely be widely applicable for improving RNP delivery using various cell-derived bioparticles, including the five distinct VLP constructs we tested in this study (Supplementary Fig. 5).

Altogether, our study provides a general workflow for identifying perturbations in producer cells that impact eVLP production and genetically engineering producer cells for improved eVLP production. While previous studies have applied CRISPR screens that use particle-packaged nucleic acid as a way to investigate the cellular determinants of viral vector^{24–26} or extracellular vesicle production^{50,51}, our study is the first to our knowledge that leverages insights from a producer-cell screen to improve VLP production and delivery potency. Notably, our results highlight the importance of conducting a producer-cell screen using RNP-packaging VLPs instead of viral vectors, since we uncovered genes that are uniquely relevant for RNP cargo expression and packaging. Additionally, our screen design is highly general and can be applied to

evaluate various genetic and epigenetic perturbations on a genome-wide scale, including for CRISPR activation or base editing screens. We anticipate that further improvements in particle production are likely possible by employing varied producer-cell perturbations instead of single gene knockouts alone. Overall, while iterative particle architecture engineering continues to improve VLP delivery potency and cell-type targeting capabilities^{10,13,22,52}, our work establishes producer-cell genetic engineering as a distinct and potentially powerful strategy for maximizing the utility of VLP-based delivery modalities.

Methods

Ethics statement

We confirm that the research in this study complies with all relevant ethical regulations and was approved by the Institutional Biosafety Committee of the Whitehead Institute for Biomedical Research. All mouse experiments were compliant with relevant ethical regulations and were approved by the MIT Committee on Animal Care (D16-00078; 2402000629).

Cloning

Plasmids used in this study were cloned via Gibson cloning (NEBuilder[®] HiFi DNA Assembly; E2621X) or Golden Gate cloning. DNA was amplified via PCR using Phusion HotStart II polymerase (Thermo Fisher Scientific; F537L). Mach1 (Thermo Fisher Scientific; C862003) or NEB[®] Stable (New England Biolabs; C3040H) chemically competent *E. coli* were used for plasmid propagation. Plasmids were isolated using QIAGEN Plasmid Plus Midi (12945) or Maxi (12963) Kits according to the manufacturer's protocols.

Cell culture

HEK293T cells (ATCC; CRL-3216), Gesicle Producer 293T cells (Takara; 632617), HEK293T/17 cells (ATCC; CRL-11268), and Neuro-2a cells (ATCC; CCL-131) were maintained in DMEM + GlutaMAX (Life Technologies; 10569044) supplemented with 10% (v/v) fetal bovine serum (Gibco; A5670701). Cells were cultured at 37 °C with 5% carbon dioxide and were confirmed to be negative for mycoplasma by testing with MycoAlert (Lonza; LT07-318).

eVLP production and purification

eVLPs were produced as described previously^{8,22}. Briefly, eVLPs were produced by transient transfection of Gesicle 293T cells, HEK293T/17 cells, or variants thereof as noted in the main text and figure legends. Producer cells were seeded in T-75 flasks at a density of 5×10^6 cells per flask in 10 mL of media. After 20–24 h, cells were transfected using the jetPRIME transfection reagent (Polyplus; 114-75) according to the manufacturer's protocols. For producing eVLPs, a mixture of plasmids expressing VSV-G (400 ng), MMLV gag-pro-pol (3375 ng), gag-cargo (1125 ng), and an sgRNA (4400 ng) was co-transfected per T-75 flask.

In all, 40–48 h post-transfection, producer cell supernatant was harvested and centrifuged for 5 min at $500 \times g$ to remove cell debris. The clarified eVLP-containing supernatant was filtered through a 0.45- μ m PVDF filter (Millipore; SE1M003M00). The filtered supernatant was concentrated 100-fold using PEG-it Virus Precipitation Solution (System Biosciences; LV825A-1) according to the manufacturer's protocols and resuspended in Opti-MEM serum-free media (Thermo Fisher Scientific; 31985070). For eVLPs prepared for protein or RNA quantification, or those that were injected into mice, the filtered supernatant was concentrated 1500-fold by ultracentrifugation using a cushion of 20% (w/v) sucrose in PBS. Ultracentrifugation was performed at 26,500 rpm ($86,242 \times g$) for 2 h (4 °C) using an SW32 Ti rotor in an Optima XE Ultracentrifuge (Beckman Coulter). Following ultracentrifugation, eVLP pellets were resuspended in cold PBS pH 7.4 (Gibco; 10010023) and centrifuged at $1000 \times g$ for 5 min to remove debris. eVLPs were frozen at a rate of -1 °C/min and stored at -80 °C. eVLPs were thawed on ice immediately prior to use.

eVLP transduction and genomic DNA isolation

Cells were transduced with eVLPs as described previously^{8,22} with a few modifications. Cells were plated for transduction in 96-well plates at a density of 16,000 cells per well. After 20–24 h, eVLPs (that were concentrated 100-fold using PEG precipitation described above) were added directly to the culture media in each well. In almost all cases, eVLPs were serially diluted by twofold to generate dose titration curves, and a constant volume of 5 μ L of eVLP-containing solution was added to each well. For certain experiments, a constant volume of 10 or 20 μ L of VLP-containing solution was added to each well, as noted in the appropriate subfigures. In all, 48–72 h post-transduction, cellular genomic DNA was isolated. Media was aspirated from each well, and 60 μ L of lysis buffer (10 mM Tris-HCl pH 8.0, 0.05% SDS, 25 μ g mL⁻¹ Proteinase K (Thermo Fisher Scientific; E00492)) was added to each well. Lysis was achieved by incubation at 37 °C for 1–1.5 h followed by heat inactivation at 80 °C for 30 min.

High-throughput sequencing of genomic DNA

Genomic DNA was isolated as described above. Following genomic DNA isolation, 1 μ L of the isolated DNA (1–10 ng) was used as input for the first of two PCR reactions. Genomic loci were amplified in PCR1 using Phusion U polymerase (Thermo Fisher Scientific; F562L). PCR1 primers are listed in Supplementary Data 2 and 7 under the HTS_forward and HTS_reverse columns. PCR1 was performed as follows: 95 °C for 3 min; 30 cycles of 95 °C for 15 s, 61 °C for 20 s, and 72 °C for 30 s; 72 °C for 1 min. PCR1 products were confirmed on a 1% agarose gel. In total, 1 μ L of PCR1 was used as an input for PCR2 to install Illumina barcodes. PCR2 was conducted for nine cycles of amplification using Phusion HotStart II polymerase (Thermo Fisher Scientific; F537L). Following PCR2, samples were pooled and gel purified in a 1% agarose gel using a QIAquick Gel Extraction Kit (Qiagen; 28704). Library concentration was quantified using the Qubit[™] dsDNA High-Sensitivity Assay Kit (Thermo Fisher Scientific; Q33230). Samples were sequenced on an Illumina MiSeq instrument (paired-end read, read 1: 200–280 cycles, read 2: 0 cycles) using an Illumina MiSeq 300 v2 Kit (Illumina).

High-throughput sequencing data analysis for gene editing experiments

Sequencing reads were demultiplexed using the MiSeq Reporter software (v2.6) (Illumina) and were analyzed using CRISPResso2 (ref. 53) (v2.3.2) as previously described⁸. Batch analysis mode (one batch for each unique amplicon and sgRNA combination analyzed) was used in all cases. Reads were filtered by minimum average quality score ($Q > 30$) prior to analysis. For analysis of base editing efficiencies, the following quantification window parameters were used: -w 20 -wc -10. Base editing efficiencies are reported as the percentage of sequencing reads containing a given base conversion at a specific position. For analysis of prime editing efficiencies, the following quantification parameters were used: -w 30 -wc -3 --discard_indel_reads. Prime editing efficiencies are reported as the number of reads aligned to the edited amplicon sequence divided by the number of reads aligned to all amplicons multiplied by 100. Prism 10 (GraphPad) was used to generate dot plots and bar plots. Amplicon sequences are provided in Supplementary Data 2 and 7.

Lentiviral vector production

Lentiviral vectors were constructed via Golden Gate cloning into the LentiCRISPRv2-Opti backbone, a gift from the Whitehead Institute Functional Genomics Platform (Addgene #163126). Plasmids were propagated in NEB[®] Stable (New England Biolabs; C3040H) chemically competent *E. coli*. Prior to lentiviral vector production, HEK293T/17 cells were maintained in antibiotic-free DMEM supplemented with 10% fetal bovine serum (v/v). On day 1, 5×10^6 cells were plated in 10 mL of media in T-75 flasks. The following day, cells were transfected with 6 μ g of VSV-G envelope plasmid, 9 μ g of psPAX2 (plasmid encoding viral

packaging proteins) and 9 μg of transfer vector plasmid diluted in 1500 μL Opti-MEM with 70 μL of FuGENE HD transfection reagent (Promega; E2312). Two days after transfection, media was centrifuged at $500\times g$ for 5 min to remove cell debris followed by filtration using a 0.45- μm PVDF vacuum filter (Millipore; SE1M003M00). The filtered supernatant was concentrated using PEG-it Virus Precipitation Solution (System Biosciences; LV825A-1) according to the manufacturer's protocols and resuspended in Opti-MEM serum-free media (Gibco; 31985070).

sgRNA library propagation

For the genome-wide knockout screen, a previously described human genome-wide sgRNA library containing 98,077 unique sgRNAs targeting 19,707 genes across the human genome³⁰ was obtained as a gift from the Whitehead Institute Functional Genomics Platform. sgRNA sequences are listed in Supplementary Data 3. Vectors contained pU6-sgRNA expression cassettes along with pEFS-Cas9-P2A-PuroR (LentiCRISPRv2-Opti backbone, Addgene #163126). The plasmid library was propagated as follows. First, electrocompetent cells were generated from NEB[®] Stable (New England Biolabs; C3040H) chemically competent *E. coli* by growing single colonies to mid-log phase in LB media containing 10 $\mu\text{g}/\text{mL}$ tetracycline and 50 $\mu\text{g}/\text{mL}$ streptomycin, collecting cells by centrifugation at $5000\times g$ for 1 min at 4 °C, washing with cold 10% (v/v) glycerol, and repeating for a total of four washes. Freshly prepared electrocompetent cells were transferred to a chilled 0.1 cm electroporation cuvette (Bio-Rad; 1652089) and mixed with the purified, assembled library plasmids. Cells were electroporated using a time-constant protocol with $t=5$ ms at 1.5 kV. Electroporated cells were recovered at 37 °C for 25 min with shaking. Recovered cells were plated onto 500 cm^2 plates containing LB media + 1.5% agar supplemented with 100 $\mu\text{g}/\text{mL}$ carbenicillin and incubated for 16 h at 37 °C. After overnight incubation, colonies were scraped into LB media and cells were collected by centrifugation. Plasmids were purified using a Plasmid Plus Maxi Kit (Qiagen; 12963) according to the manufacturer's protocols. sgRNA representation in the propagated plasmid library was confirmed via targeted amplicon sequencing.

Genome-wide knockout screen for cargo-loaded eVLP production

Lentiviral libraries were produced as described above and were concentrated ~66-fold by PEG precipitation. Gesicle cells were seeded at a density of 1.5×10^7 cells per T-175 and immediately transduced with 105 μL of concentrated lentivirus. A total of 2.4×10^8 Gesicle cells were seeded for transduction. 24 h after transduction, cells were trypsinized and reseeded at half the original density in media supplemented with 2 $\mu\text{g}/\text{mL}$ puromycin. Puromycin selection was continued for 7 days, during which time cell viability was monitored and cells were expanded upon reaching confluency. The initial multiplicity of infection (MOI) was inferred by counting surviving cells and assuming a doubling time of 24 h. Using this method, the MOI was calculated to be 0.28, corresponding to approximately 660 \times coverage of the sgRNA library. A minimum of 1×10^8 cells were carried forward each time the cells were passaged to retain overall coverage.

After cells were robustly surviving puromycin selection (~1 week), cells were seeded for eVLP production in T-75 flasks at a density of 5×10^6 cells/flask. At this time, 1×10^8 cells were collected by centrifugation, and the cell pellet was frozen at -80 °C and reserved for RNA extraction (see below). Twenty-four hours after seeding, cells were transfected using the jetPRIME transfection reagent (Polyplus; 114-75) according to the manufacturer's protocols. A mixture of pUC19 (4400 ng), VSV-G (400 ng), MMLV gag-pro-pol (3375 ng), and MMLVgag-ABE8e (1125 ng) plasmids was co-transfected per T-75 flask. 42 h post transfection, eVLPs were harvested and filtered as described above. The filtered supernatant was concentrated by sucrose-cushion ultracentrifugation as described above. Following ultracentrifugation,

eVLP pellets were resuspended in cold PBS pH 7.4 (Gibco; 10010023). Purified eVLPs were treated with DNase (Qiagen; 79254) followed by RNA extraction using the QIAmp Viral RNA Mini Kit (Qiagen; 52904) according to the manufacturer's protocols. RNA was extracted from the producer-cell pellet using QIAzol Lysis Reagent (Qiagen; 79306) according to the manufacturer's protocols. This entire process of seeding single-knockout Gesicle cells followed by eVLP production and RNA extractions was performed twice on different days for two screen replicates.

Following RNA extraction, both producer-cell and eVLP RNA were reverse transcribed using the Maxima Reverse Transcriptase (Thermo Fisher Scientific; EP0742) according to the manufacturer's protocols. Primers and other oligonucleotides used for target-primed sgRNA reverse transcription are listed in Supplementary Data 1. The RT primer was added at a final concentration of 1 μM in the RT reaction. Following incubation at 50 °C for 20 min, the template-switching oligo (TSO) was spiked into the reaction at a final concentration of 1 μM . The reaction was incubated for a further 20 min at 50 °C, and heat inactivated at 85 °C for 5 min. For producer-cell RNA only, the RT products were further processed by hydrolyzing the RNA in 0.2 M NaOH (final concentration) and heating at 90 °C for 10 min, cleaning up with the MinElute Reaction Cleanup Kit (Qiagen; 28104) according to the manufacturer's protocols, and left-sided size selection using SPRIselect (Beckman Coulter; B23317) at a 1.5 \times bead ratio to remove smaller products and residual primers. Producer-cell cDNAs were subsequently amplified for sequencing with the KAPA HiFi HotStart ReadyMix (Roche Diagnostics; 09420398001) using 2.5 μL of cDNA input per 25 μL reaction and the following conditions: 95 °C for 3 min; 20 cycles of 98 °C for 20 s, 61 °C for 20 s, and 72 °C for 30 s; 72 °C for 2 min. eVLP cDNAs were amplified for sequencing with the KAPA HiFi HotStart ReadyMix using 2.5 μL of cDNA input per 25 μL reaction and the following conditions: 95 °C for 3 min; 14 cycles of 98 °C for 20 s, 61 °C for 20 s, and 72 °C for 30 s; 72 °C for 2 min. Illumina barcodes were installed using KAPA HiFi HotStart ReadyMix using 2 μL of PCR1 input per 25 μL reaction and the following conditions: 95 °C for 3 min; 9 cycles of 98 °C for 20 s, 61 °C for 20 s, and 72 °C for 30 s; 72 °C for 2 min. Following PCR2, samples were gel purified in a 1% agarose gel using a QIAquick Gel Extraction Kit (Qiagen; 28704). Library concentration was quantified using the Qubit High-Sensitivity Assay Kit (Thermo Fisher Scientific; Q33230). Samples were sequenced on an Illumina NextSeq instrument (paired-end read, read 1: 76 cycles, read 2: 0 cycles) using an Illumina NextSeq 75-cycle High-Output v2.5 Kit (Illumina).

Genome-wide knockout screen analysis

Code used for processing sequencing reads from the genome-wide knockout screen is provided in Supplementary Data 8. Briefly, sequencing reads were demultiplexed using bcl2fastq (v2.20.0.422). Reads were trimmed using seqkit⁵⁴ (v2.6.1) to restrict analysis to the UMI and sgRNA protospacer sequences only. Then, reads were UMI-deduplicated using AmpUMI⁵⁵ and trimmed with seqkit to remove the UMI and restrict subsequent analysis to the sgRNA protospacer sequences only. Processed reads were aligned to a reference fasta file containing all sgRNA sequences using bowtie⁵⁶ (v1.3.1), and sgRNA counts were generated from alignments as previously described³⁰. Raw sgRNA counts are provided in Supplementary Data 4. MAGeCK⁵⁷ (v0.5.9.5) was used to quantify gene-level phenotypes from the sgRNA counts. Producer-cell samples were treated as "control" samples and eVLP samples were treated as "treatment" samples for the purpose of MAGeCK analysis. Median-normalized sgRNA read counts and fold changes are provided in Supplementary Data 5, and gene-level phenotypes are provided in Supplementary Data 6. For genes with a positive median \log_2 fold change, the positive MAGeCK RRA score, *P* value, and FDR were used, and for genes with a negative median \log_2 fold change, the negative MAGeCK RRA score, *P* value,

and FDR were used. Prism 10 (GraphPad) was used to generate dot plots.

Generation of knockout cell lines

To generate knockout cell lines via Cas9/sgRNA lentiviral transduction, lentiviral vectors were cloned and produced as described above. Cells were seeded in T-75 flasks at a density of 5×10^6 cells/flask and immediately transduced with 50 μ L of concentrated lentivirus. 24 h after transduction, cells were trypsinized and reseeded in media supplemented with 2 μ g/mL puromycin. Puromycin selection was continued, during which time cell viability was monitored and cells were expanded upon reaching confluency. After cells were robustly surviving puromycin selection (-1 week), cells were harvested and genotyped via targeted-amplicon high-throughput sequencing as described above to confirm gene knockout. Cell lines were regularly genotyped over time to confirm continued gene knockout.

To generate knockout cell lines via Cas9-eVLP transduction, v4 Cas9-eVLPs were produced as described above. Cells were seeded in 96-well plates at a density of 16,000 cells per well. Twenty-four hours after seeding, cells were transduced with 5 μ L of purified Cas9-eVLPs per well. 72 h after eVLP transduction, cells were harvested and genotyped via targeted-amplicon high-throughput sequencing as described above to confirm gene knockout. Cells were expanded and regularly genotyped over time to confirm continued gene knockout.

eVLP-packaged sgRNA extraction and RT-qPCR

eVLPs for RNA extraction were purified via sucrose-cushion ultracentrifugation as described above. Purified eVLPs were treated with DNase (Qiagen; 79254) followed by RNA extraction using the QIAmp Viral RNA Mini Kit (Qiagen; 52904) according to the manufacturer's protocols. Extracted RNA was reverse transcribed using SuperScriptTM III First-Strand Synthesis SuperMix (Thermo Fisher Scientific; 18080400) and an sgRNA-specific DNA primer (see Supplementary Data 1) according to the manufacturer's protocols. qPCR analysis of the resulting cDNA was performed using a QuantStudioTM 3 Real-Time PCR System (Thermo Fisher Scientific) with SYBR green dye (Lonza; 50512). The relative eVLP-packaged sgRNA abundance was calculated as $\log_2[\text{fold change}] (\Delta\Delta C_t)$ relative to control eVLPs (i.e., those produced from standard or *AAVSI*-knockout cells).

Producer-cell RNA extraction and RT-qPCR

Cellular RNA was extracted using the RNeasy Plus Mini Kit (Qiagen; 74136) according to the manufacturer's protocols. Extracted RNA was reverse transcribed using SuperScriptTM III First-Strand Synthesis SuperMix (Thermo Fisher Scientific; 18080400) using random hexamer primers according to the manufacturer's protocols. qPCR analysis of the resulting cDNA was performed using a QuantStudioTM 3 Real-Time PCR System (Thermo Fisher Scientific) with SYBR green dye (Lonza; 50512). The relative Cas9 mRNA abundance across different producer cells was calculated via the $\Delta\Delta C_t$ method using *ACTB* as the housekeeping gene. qPCR primers are listed in Supplementary Data 1.

Producer-cell protein extraction and Western blot analyses

For producer-cell protein extraction, 1×10^6 cells were collected by centrifugation at $500 \times g$ for 5 min. Cell pellets were washed once with 1 mL of cold PBS and lysed using RIPA buffer (Thermo Fisher Scientific; 89901) supplemented with cOmpleteTM protease inhibitor cocktail (Roche Diagnostics; 11836153001) according to the manufacturer's protocols. Cells were lysed at 4 °C for 30 min with gentle agitation. The lysate was clarified by centrifugation at $10,000 \times g$ for 20 min at 4 °C, and the clarified supernatant was combined with 4 \times Laemmli Sample Buffer (Bio-Rad; 1610747) and heated at 95 °C for 10 min. Protein extracts were subsequently separated by electrophoresis at 150 V for 45 min on a NuPAGE 3–8% Tris-Acetate gel (Thermo Fisher Scientific; EA0378BOX) in 1 \times NuPAGE Tris-Acetate SDS running buffer (Thermo

Fisher Scientific; LA0041). Transfer to a PVDF membrane was performed using an iBlot 2 Gel Transfer Device (Thermo Fisher Scientific) at 20 V for 7 min. The membrane was blocked for 1 h at room temperature with rocking in blocking buffer: 1% bovine serum albumin (BSA) and 0.1% Tween-20 in TBS (150 mM NaCl and 50 mM Tris-HCl). After blocking, the membrane was incubated overnight at 4 °C with rocking with mouse anti-Cas9 (Cell Signaling Technology; 14697, 1:1000 dilution) and rabbit anti-actin (Cell Signaling Technology; 4970, 1:1000 dilution). The membrane was washed three times with 1 \times TBST (150 mM NaCl, 0.5% Tween-20, and 50 mM Tris-HCl) for 10 min each time at room temperature, then incubated with goat anti-mouse secondary antibody (LI-COR IRDye 680RD; 926-68070, 1:10,000 dilution in blocking buffer) and goat anti-rabbit secondary antibody (LI-COR IRDye 800CW; 926-32211, 1:10,000 dilution in blocking buffer) for 1 h at room temperature with rocking. The membrane was washed as before and imaged using an Odyssey Imaging System (LI-COR). Protein abundances were quantified by densitometry using ImageJ (v2.14.0). Cas9 abundances were normalized to the actin abundance within each sample, and comparisons across samples were performed using these actin-normalized values.

For protein extraction from cells transfected with eVLP production plasmids, cells were first seeded for eVLP production in T-75 flasks as described above. Twenty-four hours after seeding, cells were transfected with all eVLP production plasmids except the VSV-G plasmid. 48 h after transfection, cells were trypsinized and collected by centrifugation, and were then processed as described above.

eVLP protein content quantification

eVLP protein content quantification was performed as described previously⁸. Briefly, ultracentrifuge-purified eVLPs were lysed in dye-free Laemmli sample buffer (50 mM Tris-HCl pH 7.0, 2% sodium dodecyl sulfate (SDS), 10% (v/v) glycerol, 2 mM dithiothreitol (DTT)) by heating at 95 °C for 15 min. The concentration of ABE protein in purified eVLPs was quantified using the FastScanTM Cas9 (*S. pyogenes*) ELISA kit (Cell Signaling Technology; 29666 C) according to the manufacturer's protocols. Recombinant Cas9 (*S. pyogenes*) nuclease protein (New England Biolabs; M0386) was used to generate the standard curve for quantification. The concentration of MLV p30 protein in purified eVLPs was quantified using the MuLV Core Antigen ELISA kit (Cell Biolabs; VPK-156) according to the manufacturer's protocols. To calculate eVLP titer in particles/ μ L, the p30 concentration in ng/mL determined by ELISA was multiplied by a factor 2030.57, which accounts for molarity conversions, assumes that 20% of p30 molecules in solution are associated with particles, and assumes a copy number of 1800 molecules of p30 per eVLP, as previously described⁸. The number of ABE protein molecules per eVLP was calculated by determining the ratio of Cas9 molecules to p30 molecules and assuming a copy number of 1800 molecules of p30 per eVLP, as previously described⁸.

Animal experiments

All mouse experiments were compliant with relevant ethical regulations and were approved by the MIT Committee on Animal Care (D16-00078; 2402000629). Wild-type 8-week-old adult male C57BL/6j mice (000664) were purchased from the Jackson Laboratory. Sex was not considered in the study design and analysis since it was previously demonstrated that the outcomes of eVLP-mediated liver base editing in mice are not dependent on sex⁸. All mice were housed in a room maintained on a 12 h light and dark cycle with ad libitum access to standard rodent diet and water. Animals were randomly assigned to various experimental groups.

Retro-orbital injections were performed as described previously⁸ with a few modifications. eVLPs for retro-orbital injections were purified via sucrose-cushion ultracentrifugation as described above. Immediately prior to injection, eVLPs were partially clarified by

centrifugation at $1000\times g$ for 5 min to remove debris. The eVLP-containing supernatant was diluted with 0.9% NaCl (Hospira; 00409-4888-10), and a total of 100 μL solution was injected per mouse: 85 μL saline + 15 μL of 1500-fold concentrated purified eVLPs, containing 3×10^{11} eVLPs as was quantified by ELISA using the procedure described above. Genomic DNA was purified from bulk liver tissue using the Agencourt DNAdvance kit (Beckman Coulter; A48705) according to the manufacturer's protocols. Purified genomic DNA was amplified for high-throughput sequencing as described above, with 25 cycles of amplification during PCR1.

Production of other VLP constructs

ENVLP⁺ particles¹⁰, miniEDVs⁴⁴, RIDE VLPs¹⁶, and VEDIC⁴⁵ particles were produced analogously to eVLPs. Producer cells were seeded in T-75 flasks at a density of 5×10^6 cells per flask. After 20–24 h, cells were transfected using the jetPRIME transfection reagent (Polyplus; 114-75) according to the manufacturer's protocols.

For producing ABE-ENVLP⁺ particles, a mixture of plasmids expressing VSV-G (1550 ng), psPAX2-D64V (1149 ng; Addgene #63586, a gift from David Rawlings & Andrew Scharenberg), pCMV_ENVLP⁺ (665 ng; Addgene #232427, a gift from Gil Westmeyer), pCMV_ABE8e₂-superNLS (1023 ng; Addgene #232429, a gift from Gil Westmeyer), and a *BCL11A*-targeting PP7-containing sgRNA (4913 ng; cloned from Addgene #232432, a gift from Gil Westmeyer) was co-transfected per T-75 flask.

For producing PE-ENVLP⁺ particles, a mixture of plasmids expressing VSV-G (1550 ng), psPAX2-D64V (1149 ng; Addgene #63586, a gift from David Rawlings & Andrew Scharenberg), pCMV_ENVLP⁺ (665 ng; Addgene #232427, a gift from Gil Westmeyer), pCMV_iPE-C_P2A_Csy4 (1023 ng; Addgene #232428, a gift from Gil Westmeyer), and pU6_HEK3+IT > A_PP7-C4-Q1 (4913 ng; Addgene #232437, a gift from Gil Westmeyer) was co-transfected per T-75 flask.

For producing miniEDVs, a mixture of plasmids expressing VSV-G (930 ng), a *BCL11A*-targeting sgRNA and miniGag (2790 ng; cloned from Addgene #228957, a gift from Jennifer Doudna), and a *BCL11A*-targeting sgRNA and miniGag-Cas9 (5580 ng; cloned from Addgene #228958, a gift from Jennifer Doudna) was co-transfected per T-75 flask.

For producing RIDE VLPs, a mixture of plasmids expressing VSV-G (760 ng), pRSV-Rev (610 ng; Addgene #12253, a gift from Didier Trono), pMS2M-PH-gagpol-D64V (1320 ng; Addgene #166031, a gift from Yujia Cai), pMDLg/pRRE (1320 ng; Addgene #12251, a gift from Didier Trono), ABE8e (2640 ng; Addgene #138489, a gift from David Liu), and a *BCL11A*-targeting MS2-containing sgRNA (2640 ng; Addgene #229772, a gift from Yujia Cai) was co-transfected per T-75 flask.

For producing VEDIC particles, a mixture of plasmids expressing VSV-G (400 ng), a CD63-intein-Cas9 fusion (3500 ng), and *HEK2*-targeting sgRNA (5400 ng) was co-transfected per T-75 flask.

For all VLPs, 40–48 h post-transfection, producer cell supernatant was harvested and centrifuged for 5 min at $500\times g$ to remove cell debris. The clarified VLP-containing supernatant was filtered through a 0.45- μm PVDF filter (Millipore; SE1M003M00). The filtered supernatant was concentrated 100-fold using PEG-it Virus Precipitation Solution (System Biosciences; LV825A-1) according to the manufacturer's protocols and resuspended in Opti-MEM serum-free media (Thermo Fisher Scientific; 31985070). For all VLPs, transduction of HEK293T cells was performed as described above for eVLPs.

Quantification of eVLP-packaged Cas9 molecules complexed with sgRNAs

For each construct, the number of Cas9 molecules per unit volume of eVLPs was calculated via anti-Cas9 ELISA as described above. For sgRNA quantification, purified eVLPs were treated with DNase (Qiagen; 79254). Then, 100 ng of 151-bp spike-in RNA (see below) was added to each sample, followed by RNA extraction using the QIAmp Viral RNA

Mini Kit (Qiagen; 52904) according to the manufacturer's protocols. Extracted RNA was reverse transcribed using SuperScriptTM III First-Strand Synthesis SuperMix (Thermo Fisher Scientific; 18080400) and both an sgRNA-specific DNA primer and a spike-in RNA-specific DNA primer (see Supplementary Data 1) according to the manufacturer's protocols. qPCR analysis of the resulting cDNA was performed with both sgRNA-specific and spike-in RNA-specific primers (see Supplementary Data 1) using a QuantStudioTM 3 Real-Time PCR System (Thermo Fisher Scientific) with SYBR green dye (Lonza; 50512).

To determine the absolute amount of sgRNA and spike-in cDNA in each sample, a standard curve for each cDNA species was generated. First, RNA standards for both species were generated via *in vitro* transcription using the HiScribe[®] T7 Quick High Yield RNA Synthesis Kit (New England Biolabs; E2050S). Transcribed RNA yield was quantified using the QubitTM RNA High-Sensitivity Assay Kit (Thermo Fisher Scientific; Q32852). Then, serial dilutions of each RNA standard were made in water, and the resulting diluted RNAs were subjected to reverse transcription using either sgRNA-specific or spike-in RNA-specific DNA primers as described above. The resulting cDNAs were used as input into qPCR reactions to generate a standard curve for each cDNA species.

Standard curves were analyzed via linear regression using Prism 10 (GraphPad), and these curves were used to calculate the number of sgRNA and spike-in RNA molecules present in each eVLP-derived sample after RNA extraction. To determine the number of sgRNA molecules present in each eVLP sample before RNA extraction, RNA loss during the extraction process was accounted for by calculating the percent recovery of spike-in RNA for each sample (using the knowledge that exactly 100 ng of spike-in RNA was added to each sample before RNA extraction, as described above). Using this RNA recovery factor, the number of sgRNA molecules present in each eVLP sample before RNA extraction was calculated (with the assumption that, for each sample, the percent recovery of spike-in RNA and sgRNA are equal since both species are of similar size). Finally, the percentage of eVLP-packaged Cas9 molecules complexed with sgRNAs was calculated for each sample by dividing the number of sgRNA molecules per unit volume of eVLPs by the number of Cas9 molecules per unit volume of eVLPs. This calculation assumes that all sgRNA molecules detected in eVLPs are complexed with Cas9 molecules, since sgRNA packaging into eVLPs in the absence of Cas9 is negligible²².

Statistics and reproducibility

Data are presented as mean and standard deviation (s.d.). No statistical methods were used to predetermine sample size. No data were excluded from analyses. The experiments were not randomized. The investigators were not blinded to allocation during experiments and outcome assessment. Statistical analysis was performed using Prism 10 (GraphPad). Sample sizes are described in the figure legends.

Reporting summary

Further information on research design is available in the Nature Portfolio Reporting Summary linked to this article.

Data availability

The high-throughput sequencing data generated in this study have been deposited at the NCBI Sequence Read Archive database under accession code [PRJNA1288558](https://www.ncbi.nlm.nih.gov/sra/PRJNA1288558). Raw data from the genome-wide knockout screen is provided in Supplementary Data 3–6. Source data are provided with this paper.

Code availability

The code used for analyzing base editing efficiencies is available at <https://github.com/pinelloblab/CRISPResso2>. The code used for analyzing CRISPR screen results is available in Supplementary Data 8 and at <https://sourceforge.net/p/mageck/wiki/Home/>.

References

- Raguram, A., Banskota, S. & Liu, D. R. Therapeutic in vivo delivery of gene editing agents. *Cell* **185**, 2806–2827 (2022).
- van Haasteren, J., Li, J., Scheideler, O. J., Murthy, N. & Schaffer, D. V. The delivery challenge: fulfilling the promise of therapeutic genome editing. *Nat. Biotechnol.* **38**, 845–855 (2020).
- Wang, D., Zhang, F. & Gao, G. CRISPR-based therapeutic genome editing: strategies and in vivo delivery by AAV vectors. *Cell* **181**, 136–150 (2020).
- Wei, T. et al. Delivery of tissue-targeted scalpels: opportunities and challenges for in vivo CRISPR/Cas-based genome editing. *ACS Nano* **14**, 9243–9262 (2020).
- Wang, J. Y. & Doudna, J. A. CRISPR technology: a decade of genome editing is only the beginning. *Science* **379**, eadd8643 (2023).
- Tsuchida, C. A., Wasko, K. M., Hamilton, J. R. & Doudna, J. A. Targeted nonviral delivery of genome editors in vivo. *Proc. Natl. Acad. Sci. USA* **121**, e2307796121 (2024).
- An, M. et al. Engineered virus-like particles for transient delivery of prime editor ribonucleoprotein complexes in vivo. *Nat. Biotechnol.* **42**, 1526–1537 (2024).
- Banskota, S. et al. Engineered virus-like particles for efficient in vivo delivery of therapeutic proteins. *Cell* **185**, 250–265.e216 (2022).
- Choi, J. G. et al. Lentivirus pre-packed with Cas9 protein for safer gene editing. *Gene Ther.* **23**, 627–633 (2016).
- Geilenkeuser, J. et al. Engineered nucleocytoplasmic vehicles for loading of programmable editors. *Cell* **188**, 2637–2655.e2631 (2025).
- Haldrup, J. et al. Engineered lentivirus-derived nanoparticles (LVNPs) for delivery of CRISPR/Cas ribonucleoprotein complexes supporting base editing, prime editing and in vivo gene modification. *Nucleic Acids Res.* **51**, 10059–10074 (2023).
- Halegua, T. et al. Delivery of Prime editing in human stem cells using pseudoviral NanoScribes particles. *Nat. Commun.* **16**, 397 (2025).
- Hamilton, J. R. et al. In vivo human T cell engineering with enveloped delivery vehicles. *Nat. Biotechnol.* **42**, 1684–1692 (2024).
- Hamilton, J. R. et al. Targeted delivery of CRISPR-Cas9 and transgenes enables complex immune cell engineering. *Cell Rep.* **35**, 109207 (2021).
- Indikova, I. & Indik, S. Highly efficient ‘hit-and-run’ genome editing with unconcentrated lentivectors carrying Vpr.Prot.Cas9 protein produced from RRE-containing transcripts. *Nucleic Acids Res.* **48**, 8178–8187 (2020).
- Ling, S. et al. Customizable virus-like particles deliver CRISPR-Cas9 ribonucleoprotein for effective ocular neovascular and Huntington’s disease gene therapy. *Nat. Nanotechnol.* **20**, 543–553 (2025).
- Lu, Z. et al. Lentiviral capsid-mediated *Streptococcus pyogenes* Cas9 ribonucleoprotein delivery for efficient and safe multiplex genome editing. *CRISPR J.* **4**, 914–928 (2021).
- Lyu, P., Javidi-Parsijani, P., Atala, A. & Lu, B. Delivering Cas9/sgRNA ribonucleoprotein (RNP) by lentiviral capsid-based bionanoparticles for efficient ‘hit-and-run’ genome editing. *Nucleic Acids Res.* **47**, e99 (2019).
- Lyu, P. et al. Adenine base editor ribonucleoproteins delivered by lentivirus-like particles show high on-target base editing and undetectable RNA off-target activities. *CRISPR J.* **4**, 69–81 (2021).
- Lyu, P., Wang, L. & Lu, B. Virus-like particle mediated CRISPR/Cas9 delivery for efficient and safe genome editing. *Life* **10**, 366 (2020).
- Mangeot, P. E. et al. Genome editing in primary cells and in vivo using viral-derived Nanoblades loaded with Cas9-sgRNA ribonucleoproteins. *Nat. Commun.* **10**, 45 (2019).
- Raguram, A., An, M., Chen, P. Z. & Liu, D. R. Directed evolution of engineered virus-like particles with improved production and transduction efficiencies. *Nat. Biotechnol.* **43**, 1635–1647 (2025).
- Xu, D. et al. Programmable epigenome editing by transient delivery of CRISPR epigenome editor ribonucleoproteins. *Nat. Commun.* **16**, 7948 (2025).
- Barnes, C. R. et al. Genome-wide activation screens to increase adeno-associated virus production. *Mol. Ther. Nucleic Acids* **26**, 94–103 (2021).
- Iaffaldano, B. J., Marino, M. P. & Reiser, J. CRISPR library screening to develop HEK293-derived cell lines with improved lentiviral vector titers. *Front. Genome Ed.* **5**, 1218328 (2023).
- O’Driscoll, E. E., Arora, S., Lang, J. F., Davidson, B. L. & Shalem, O. CRISPR screen reveals modifiers of rAAV production including known rAAV infection genes playing an unexpected role in vector production. *Mol. Ther. Methods Clin. Dev.* **33**, 101408 (2025).
- Tridgett, M. et al. Lentiviral vector packaging and producer cell lines yield titers equivalent to the industry-standard four-plasmid process. *Mol. Ther. Methods Clin. Dev.* **32**, 101315 (2024).
- Han, J., Tam, K., Tam, C., Hollis, R. P. & Kohn, D. B. Improved lentiviral vector titers from a multi-gene knockout packaging line. *Mol. Ther. Oncolytics* **23**, 582–592 (2021).
- Xinyue, Z. et al. Engineering of HEK293T cell factory for lentiviral production by high-throughput selected genes. *CRISPR J.* **7**, 272–282 (2024).
- Lam, B. et al. Multi-species genome-wide CRISPR screens identify conserved suppressors of cold-induced cell death. *eLife* <https://doi.org/10.7554/eLife.102310.102311> (2024).
- Replogle, J. M. et al. Combinatorial single-cell CRISPR screens by direct guide RNA capture and targeted sequencing. *Nat. Biotechnol.* **38**, 954–961 (2020).
- Seczynska, M., Bloor, S., Cuesta, S. M. & Lehner, P. J. Genome surveillance by HUSH-mediated silencing of intronless mobile elements. *Nature* **601**, 440–445 (2022).
- Seczynska, M. & Lehner, P. J. The sound of silence: mechanisms and implications of HUSH complex function. *Trends Genet.* **39**, 251–267 (2023).
- DeKolver, R. C. et al. Functional genomics, proteomics, and regulatory DNA analysis in isogenic settings using zinc finger nuclease-driven transgenesis into a safe harbor locus in the human genome. *Genome Res.* **20**, 1133–1142 (2010).
- Liao, J. et al. Therapeutic adenine base editing of human hematopoietic stem cells. *Nat. Commun.* **14**, 207 (2023).
- Johnson, S. S., Zhang, C., Fromm, J., Willis, I. M. & Johnson, D. L. Mammalian Maf1 is a negative regulator of transcription by all three nuclear RNA polymerases. *Mol. Cell* **26**, 367–379 (2007).
- Vannini, A. et al. Molecular basis of RNA polymerase III transcription repression by Maf1. *Cell* **143**, 59–70 (2010).
- Vorlander, M. K. et al. Structural basis for RNA polymerase III transcription repression by Maf1. *Nat. Struct. Mol. Biol.* **27**, 229–232 (2020).
- Musunuru, K. et al. In vivo CRISPR base editing of PCSK9 durably lowers cholesterol in primates. *Nature* **593**, 429–434 (2021).
- Levy, J. M. et al. Cytosine and adenine base editing of the brain, liver, retina, heart and skeletal muscle of mice via adeno-associated viruses. *Nat. Biomed. Eng.* **4**, 97–110 (2020).
- Bauler, M. et al. Production of lentiviral vectors using suspension cells grown in serum-free media. *Mol. Ther. Methods Clin. Dev.* **17**, 58–68 (2020).
- Richter, M. F. et al. Phage-assisted evolution of an adenine base editor with improved Cas domain compatibility and activity. *Nat. Biotechnol.* **38**, 883–891 (2020).
- Neugebauer, M. E. et al. Evolution of an adenine base editor into a small, efficient cytosine base editor with low off-target activity. *Nat. Biotechnol.* **41**, 673–685 (2023).
- Ngo, W. et al. Mechanism-guided engineering of a minimal biological particle for genome editing. *Proc. Natl. Acad. Sci. USA* **122**, e2413519121 (2025).
- Liang, X. et al. Engineering of extracellular vesicles for efficient intracellular delivery of multimodal therapeutics including genome editors. *Nat. Commun.* **16**, 4028 (2025).

46. Chen, Y. H. et al. Rapid lentiviral vector producer cell line generation using a single DNA construct. *Mol. Ther. Methods Clin. Dev.* **19**, 47–57 (2020).
47. Lee, Z., Lu, M., Irfanullah, E., Soukup, M. & Hu, W. S. Construction of an rAAV producer cell line through synthetic biology. *ACS Synth. Biol.* **11**, 3285–3295 (2022).
48. Powers, A. D., Drury, J. E., Hoehamer, C. F., Lockey, T. D. & Meagher, M. M. Lentiviral vector production from a stable packaging cell line using a packed bed bioreactor. *Mol. Ther. Methods Clin. Dev.* **19**, 1–13 (2020).
49. Montagna, C. et al. VSV-G-enveloped vesicles for traceless delivery of CRISPR-Cas9. *Mol. Ther. Nucleic Acids* **12**, 453–462 (2018).
50. Kunitake, K. et al. Barcoding of small extracellular vesicles with CRISPR-gRNA enables comprehensive, subpopulation-specific analysis of their biogenesis and release regulators. *Nat. Commun.* **15**, 9777 (2024).
51. Lu, A. et al. Genome-wide interrogation of extracellular vesicle biology using barcoded miRNAs. *eLife* **7**, e41460 (2018).
52. Streibinger, D. et al. Cell type-specific delivery by modular envelope design. *Nat. Commun.* **14**, 5141 (2023).
53. Clement, K. et al. CRISPResso2 provides accurate and rapid genome editing sequence analysis. *Nat. Biotechnol.* **37**, 224–226 (2019).
54. Shen, W., Le, S., Li, Y. & Hu, F. SeqKit: a cross-platform and ultrafast toolkit for FASTA/Q file manipulation. *PLoS One* **11**, e0163962 (2016).
55. Clement, K., Farouni, R., Bauer, D. E. & Pinello, L. AmpUMI: design and analysis of unique molecular identifiers for deep amplicon sequencing. *Bioinformatics* **34**, i202–i210 (2018).
56. Langmead, B., Trapnell, C., Pop, M. & Salzberg, S. L. Ultrafast and memory-efficient alignment of short DNA sequences to the human genome. *Genome Biol.* **10**, R25 (2009).
57. Li, W. et al. MAGeCK enables robust identification of essential genes from genome-scale CRISPR/Cas9 knockout screens. *Genome Biol.* **15**, 554 (2014).

Acknowledgements

This work was supported by the Whitehead Institute and Whitehead Fellows Program (A.R.); NIH Director's Early Independence Award DP5OD037342 (A.R.); Merkin Institute for Transformative Technologies in Healthcare (A.R.); McGuire Family Foundation (A.R.); James M. and Cathleen D. Stone Foundation (A.R.); Owens Family Foundation (A.R.); and Valhalla Foundation (A.R.). H.J. acknowledges support from the National Research Foundation of Korea. A.S. was supported by the Whitehead Scholars Program at Williams College. We thank H. Keys and the Functional Genomics Platform at Whitehead Institute for providing the genome-wide sgRNA library used in our study; A. Nelson, D. Liu, and the Whitehead Genome Technology Core for generous access to Illumina sequencing instrumentation; and the Jain, Reddien, Weissman, and Young Labs for generous access to equipment.

Author contributions

A.R. conceived the project. D.L., H.J., A.G., A.S., and A.R. designed the research, performed experiments, and analyzed data. H.J. performed mouse experiments. A.R. wrote the manuscript, and all authors edited the manuscript.

Competing interests

The authors declare the following competing financial interests: D.L. and A.R. through the Whitehead Institute have submitted a patent application to the United States Patent Office pertaining to the engineered producer cells described in this work (US Application No. 63/798,416). The remaining authors declare no competing interests.

Additional information

Supplementary information The online version contains supplementary material available at <https://doi.org/10.1038/s41467-026-71925-8>.

Correspondence and requests for materials should be addressed to Aditya Raguram.

Peer review information *Nature Communications* thanks Dong-Jiunn Truong and the other, anonymous, reviewer(s) for their contribution to the peer review of this work. A peer review file is available.

Reprints and permissions information is available at <http://www.nature.com/reprints>

Publisher's note Springer Nature remains neutral with regard to jurisdictional claims in published maps and institutional affiliations.

Open Access This article is licensed under a Creative Commons Attribution-NonCommercial-NoDerivatives 4.0 International License, which permits any non-commercial use, sharing, distribution and reproduction in any medium or format, as long as you give appropriate credit to the original author(s) and the source, provide a link to the Creative Commons licence, and indicate if you modified the licensed material. You do not have permission under this licence to share adapted material derived from this article or parts of it. The images or other third party material in this article are included in the article's Creative Commons licence, unless indicated otherwise in a credit line to the material. If material is not included in the article's Creative Commons licence and your intended use is not permitted by statutory regulation or exceeds the permitted use, you will need to obtain permission directly from the copyright holder. To view a copy of this licence, visit <http://creativecommons.org/licenses/by-nc-nd/4.0/>.

© The Author(s) 2026